

Experimental Observations on the Effect of Load History on Performance Limit States of Circular Bridge Columns

J.C. Goodnight, M.J. Kowalsky, and J.M. Nau

North Carolina State University, United States



15 WCEE
LISBOA 2012

SUMMARY:

In this paper, the importance of displacement history and its effects on performance limit states, the relationship between strain and displacement, and the spread of plasticity in reinforced concrete structures is explored. An experimental study is currently underway to assess the performance of thirty circular, well-confined, bridge columns subjected to various unidirectional displacement histories including monotonic, reversed cyclic, and earthquake time-history response. The test variables include load history, transverse reinforcement detailing, axial load ratio, aspect ratio, and longitudinal steel content. Longitudinal reinforcing bars were instrumented to obtain strain hysteresis, vertical strain profiles, cross section curvatures, curvature distributions, and fixed-end rotations attributable to strain penetration.

Keywords: Load History, Performance Limit States, and Bar Buckling

1. INTRODUCTION

The goal of performance based seismic engineering is to design structures to achieve a specific level of performance under a specific earthquake hazard within definable levels of reliability, as defined by the SEAOC (1999). To satisfy the aims of performance based design, levels of damage which interrupt the serviceability of the structure or require more invasive repair techniques must be related to engineering criteria. For reinforced concrete flexural member such as bridge columns, concrete compressive and steel tensile strain limits are the best indicators of damage. Closely spaced transverse steel hoops or spirals provide adequate confinement and shear resistance to produce a flexural mode of failure for columns with modern detailing. An understanding of the spread of plasticity in reinforced concrete structures is required to determine the deformation at damage limit states.

Serviceability limit states such as concrete cover crushing or residual crack widths exceeding 1mm may occur during smaller, more frequent earthquakes, (Priestley, Seible, and Calvi (1996)). While the serviceability limit states do not pose a safety concern, the hinge regions must be repaired to prevent corrosion of internal reinforcing steel. At higher ductility demands produced by larger less frequent earthquakes, reinforcing bar buckling may lead to permanent elongation in the transverse steel, which diminishes its effectiveness in confining the concrete core. Bar buckling and significant damage to the core concrete represent the damage control limit states, which when exceeded lead to significant repair or replacement costs. Rupture of previously buckled bars during subsequent cycles of loading may lead to significant strength loss. The life safety or collapse prevention limit state is characterized by fracture of previously buckled bars under displacements exceeding those required to initiate bar buckling.

Previous experimental studies on circular bridge columns have shown that reinforcing bar buckling is influenced by displacement history: (Moyer and Kowalsky (2003)), (Kunnath et al. (1997)), and (Freytag (2006)). According to (Kunnath et al. (1997)), random displacement cycles provide a better means for understanding the effects of cumulative damage and assessing the performance of structures subjected to low-cycle fatigue. Analytical studies by (Syntzirma, Pantazopoulou, and Aschheim (2010)) concluded that when flexural members are controlled by bar buckling, the deformation

capacity cannot be defined uniquely since it is a function of the applied cyclic deformation history.

1.1. Test setup

While the progression of damage in flexural bridge columns has been thoroughly investigated in the past, to the author's knowledge, none of the previous studies had the ability to measure strains at the level of the reinforcement throughout the entire range of response. The goal of the experimental program presented in this paper is to investigate the impact of load history and other design variables on the relationship between strain and displacement, performance strain limits, and the spread of plasticity. The specimen was designed to represent a single degree of freedom bridge column subjected to lateral and axial load, Fig 1.1. The test specimen consists of a footing, column, and loading cap. The footing is a capacity protected member which secures the specimen to the lab strong floor using post tensioned bars. A 980kN hydraulic actuator, with a 1016mm stroke capacity, applies lateral load to the loading cap of the specimen. A spreader beam, two hydraulic jacks, and a load cell are placed above the loading cap to apply a constant axial compressive load.

The first twelve specimens contained identical geometry and reinforcement and were subjected to different quasi-static top-column displacement histories. The 610mm diameter bridge columns contained 16 #6 (19mm) A706 bars for longitudinal reinforcement ($A_{st}/A_g = 1.6\%$) and a #3 (9.5mm) A706 spiral at 51mm on center ($4A_{sp}/(D's) = 1\%$). The effect of transverse steel detailing on restraint of longitudinal bars was the main variable for Tests 13-18. The same column geometry and longitudinal reinforcement were utilized with variable spiral detailing. To this point, all of the columns tested were subjected to a constant axial load of 756kN ($P/(f'_c A_g) \approx 5\%$) and had a cantilever aspect ratio of four.

Aspect ratio and axial load ratio are the main variables for the current phase of specimens under construction, 19-24. The 457mm diameter bridge column contains 10 #6 (19mm) A706 bars for longitudinal reinforcement ($A_{st}/A_g = 1.7\%$) and a #3 (9.5mm) A706 spiral at 51mm on center ($4A_{sp}/(D's) = 1.3\%$). Future tests in the research program, 25-30, will focus on longitudinal steel content and axial load ratio. Upon completion of the experimental program, all of the variables found to be statistically significant towards describing bar buckling in an experimental column dataset by (Berry and Eberhard (2005)) will have appeared within the test matrix.

1.2. Instrumentation

The experimental program utilized an innovative instrumentation method to measure large strains at the level of the reinforcement with multiple Optotrak Certus HD 3D position monitors. The Optotrak system can read the location of target markers placed on the specimen in three dimensional space during a test. By calculating the change in three dimensional distances between target markers, strains can be determined with respect to the original unloaded gage lengths. Longitudinal reinforcement in extreme fiber regions was instrumented to obtain strain hysteresis, vertical strain profiles, cross section curvatures, curvature distributions, and fixed-end rotations attributable to strain penetration. Strain gages were applied to layers of transverse steel overlaying the longitudinal reinforcement to observe the interaction between compressive demand, transverse steel strain, and anti-buckling restraint. The discussion in this paper is related to the instrumentation method utilizing two Optotrak position monitors, Tests 8+, with target markers directly applied to six longitudinal reinforcing bars as shown in Fig. 1.1.

The top column displacement was obtained through a string potentiometer placed at the center of the lateral load. The lateral load and stroke of the 980kN hydraulic actuator were measured through an integrated load cell and LVDT. An axial load cell measured the contribution of one hydraulic jack to the total axial load of the column. A self-regulating axial load system was utilized with a third hydraulic jack in a force controlled MTS machine to regulate the pressure, and thus the load, of two jacks on top of the specimen to maintain a constant axial load throughout testing.

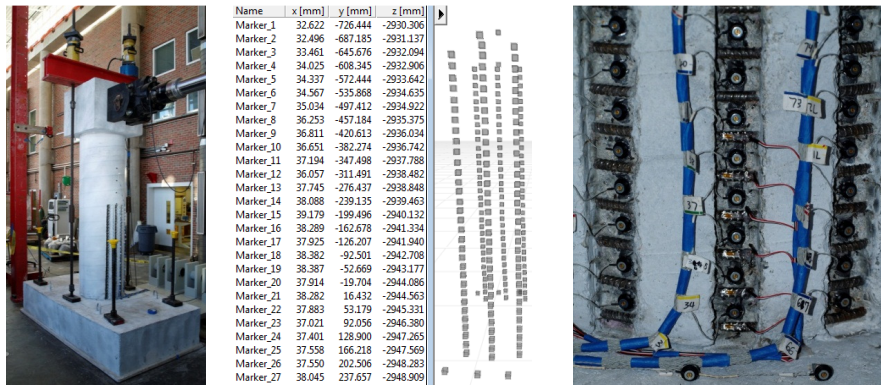


Figure 1.1. Test Setup, Target Marker Application to the Longitudinal Steel, and Optotrak Output

1.3 Loading Protocol

The specimens were subjected to various unidirectional displacement histories including monotonic, reversed cyclic, and earthquake time-history response. All of the tests utilized a quasi-static displacement controlled loading procedure. The monotonic load history included a single push cycle to failure which occurred when extreme tensile reinforcement ruptured without prior buckling on the compression side. The symmetric three cycle set laboratory load history is used to evaluate the seismic performance of structural components. The load history begins with elastic cycles to the following increments of the analytically predicted first yield force: $\frac{1}{4} F_y'$, $\frac{1}{2} F_y'$, $\frac{3}{4} F_y'$, and F_y' . The experimental first yield displacement is the average of the recorded displacements during the first yield push and pulls cycles. The equivalent yield displacement, used to determine the displacement ductility levels ($\mu_{\Delta 1} = 1 * \Delta_y$), is then calculated as $\Delta_y = \Delta_y'(M_n/M_y')$. The symmetric three cycle set load history resumes with three balanced cycles at each of the following ductility levels: 1, 1.5, 2, 3, 4, 6, 8, 10, 12, etc.

For earthquake time-history tests, the analytical top column displacement history is determined using numerical analysis in OpenSees with a force-based fiber element (Scott and Fenves (2006)) to model the column and a zero-length strain penetration element (Zhao and Sritharan (2007)). For more information on the numerical simulation of the bridge columns, refer to the companion paper by (Feng, Kowalsky, and Nau (2012)). The original acceleration input is multiplied by a constant scale factor to produce a peak displacement response suitable for the experimental test. Specific earthquake time-history response characteristics were chosen including: the number and amplitude of cycles prior to the peak, degree of symmetry, and peak displacement in each direction of loading. A separate symmetric three cycle set load history was conducted prior to earthquake time-history tests to establish the displacement ductility levels which were later verified by measured strains at the first yield displacement.

2. EXPERIMENTAL RESULTS

2.1 Damage Observations

Past research by (Moyer and Kowalsky (2003)) suggests that reinforcement buckling occurs after reversal from a peak tensile strain, while the bar is still under net elongation but compressive stress. After reversal from the peak displacement, the cracks on the tensile side begin to close, and before the column reaches zero displacement the reinforcement enters a state of compressive stress but net elongation. It is during this time, while the cracks are still open, that the reinforcement is the sole source of compression zone stability and the bars are prone to buckling. Once the cracks have closed and the concrete is reengaged, the reinforcement is unlikely to buckle.

The deformation capacity of all of the cyclically loaded specimens was limited by reinforcement bar buckling and subsequent rupture during later cycles of the load history. The following sequence of damage was observed for all of the cyclically loaded specimens: cracking, longitudinal reinforcement yield, cover concrete crushing, yielding of transverse steel, bar buckling, and then reinforcement rupture. Rupture of transverse steel was never observed. The first significant loss of strength occurred when previously buckled reinforcement ruptured in tension.

2.2 Case Study – Kobe 1995 Earthquake Record

A case study for the Kobe 1995 earthquake record is presented to explain the influence of load history on accumulated strains in the longitudinal and transverse steel. The acceleration input of the Kobe record was multiplied by 1.13 to produce an analytical top column response equivalent to displacement ductility 9.9, as shown in Fig. 2.1. A 610mm diameter bridge column, with a #3 (9.5mm) spiral at 51mm on center, was subjected to a quasi-static loading procedure which recreated the analytical Kobe displacement history and a constant axial load equivalent to $(P/(f'_c A_g) = 6.2\%)$. The test began with a small pull cycle followed by a near monotonic push to the peak displacement ductility of 9.9. The North longitudinal reinforcement, shown in Fig. 2.2, is placed into tension during push cycles while the South side is subjected to compression, refer to Fig. 2.3. The push cycle to displacement ductility 9.9 resulted in a peak tensile strain of 0.059 in the North extreme fiber bar, a peak compressive strain of -0.037 in the South extreme fiber bar, and two layers of inelastic transverse steel in the compression zone. The particular gage lengths depicted in Fig. 2.2 and Fig. 2.3 do not align with the peak tensile and compressive strains, but rather with the location of outward buckling observed later in the displacement history. The peak tensile strain of 0.059 was not sufficient to buckle the North bar during the subsequent reversal to displacement ductility -6.1.

At displacement ductility -6.1, tensile strains in the South bar reached 0.033, compressive strains in the North bar measured -0.0119, and the transverse steel on the North side of the specimen remained elastic. This peak tensile strain, combined with multiple layers of inelastic transverse steel restraint, was sufficient to buckle the South extreme fiber bar after reversal of loading. At this time, the measured strains in the South bar no longer represent engineering strains due to the outward buckled deformation between target markers. As the South bar buckles outwards, the strain in the transverse steel restraint begins to rapidly increase as shown in Fig. 2.3. The North extreme fiber bar buckled after reversal from the push cycle which ended at displacement ductility 9.3. The outward buckled deformation in the North bar caused measured strains in the transverse steel restraint to sharply increase as shown in Fig 2.2. Prior to buckling of the North extreme fiber bar, the transverse steel restraint remained elastic.

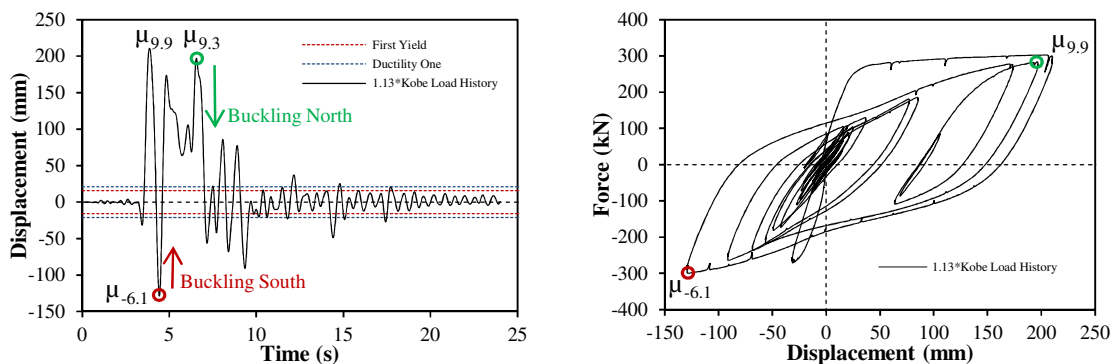


Figure 2.1. (Left) Top Column Displacement History for the Kobe 1995 Earthquake Load History and (Right) Lateral Force vs. Top Column Displacement Hysteresis for the Kobe Load History

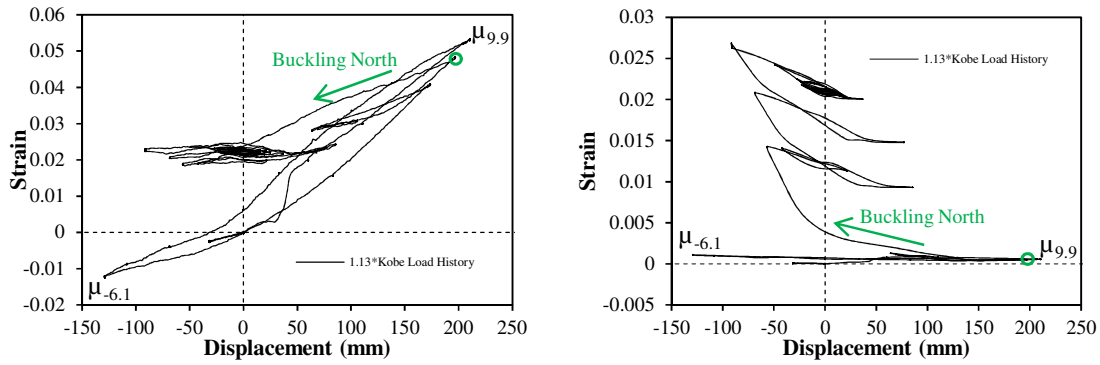


Figure 2.2. (Left) Longitudinal Steel Strain Hysteresis for the North Extreme Fiber Bar and (Right) Transverse Steel Strain Hysteresis for Spiral Layer Overlaying Outward Buckled Region of North Bar

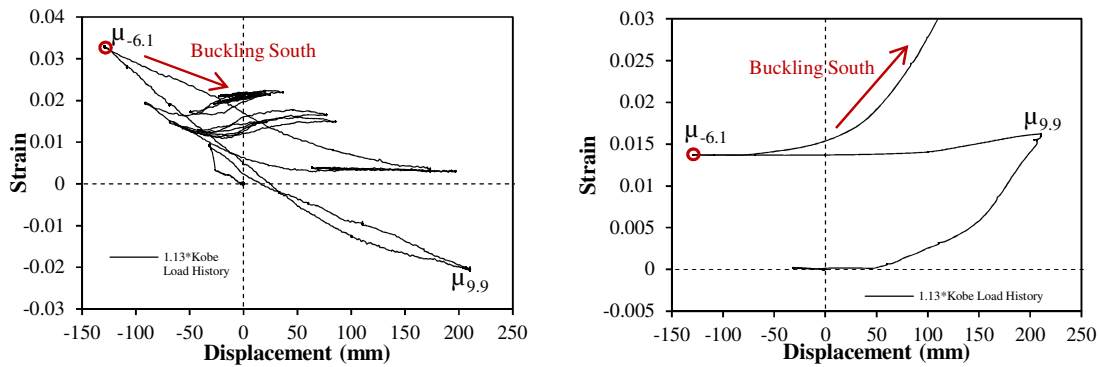


Figure 2.3. (Left) Longitudinal Steel Strain Hysteresis for the South Extreme Fiber Bar and (Right) Transverse Steel Strain Hysteresis for Spiral Layer Overlaying Outward Buckled Region of South Bar

2.2 Load History and Accumulated Strains

The main impact of load history on column behavior is its effect on accumulated strains within the longitudinal and transverse reinforcement. Inelastic strains in the transverse steel, caused by large concrete compressive demand, can decrease its effectiveness in restraining buckling of the longitudinal bars. Load histories with compressive demand sufficient to produce inelastic transverse steel may require lower values of peak tensile strain to buckle reinforcing bars after reversal of load. The symmetric three cycle set load history is more severe than the load histories produced by actual earthquakes, when evaluated to the same peak displacement, due to the balanced repeated cycles at each ductility level. Multiple cycles at the same amplitude allow each side of the specimen to be subjected to the peak compressive and tensile cycles. This creates the worst situation for a given peak displacement, the possibility if inelastic transverse steel restraint and tensile strains sufficient to buckle reinforcing bars after reversal of loading.

The relationship between strain and displacement during the largest push cycle of each load history variable test appears in Fig. 2.4. The 610mm diameter bridge columns contained a #3 (19mm) spiral at either 51mm or 38mm on center. A specimen with each transverse steel detailing was subjected to a symmetric three cycle set load history which produced bar buckling during the repeated cycles at displacement ductility eight. The following four earthquake load histories: Chichi 1999, Chile 2010, Lolleo 1985, and Darfield 2010 were scaled to produce peak response displacement ductility of 8.8, 8.7, 9.0, and 9.0 respectively. The longitudinal steel placed into tension during the peak cycle of these four load histories did not buckle during the earthquake record. For the case of the Darfield 2010 load history, the peak push displacement caused layers of transverse steel to go inelastic, and the following pull cycle to displacement ductility -7.3 had sufficient tensile strains to buckle the reinforcement after reversal. The four specimens were then subjected to symmetric three cycle set aftershock load

histories to determine the post-earthquake performance of the columns. Reinforcement buckling occurred during cycles at displacement ductility six of the cyclic aftershock studies after the Chichi 1999, Chile 2010, and Lollole 1985 load histories. The cyclic aftershock conducted after the Darfield 2010 record ruptured the previously buckled reinforcement during ductility six. To produce buckling after reversal from the peak displacement response of earthquake load histories, the Kobe 1995 and Japan 2011 records were scaled to displacement ductility 9.9 and 10 respectively.

The relationship between strain and displacement during the peak cycle does not appear to be affected by seismic load history. The buckling damage control steel tensile strain limit is influenced by load history, and previously inelastic layers of transverse steel are less effective at restraining bar buckling. At low ductility levels the measured tensile strains during the Kobe 1995 and Darfield 2010 peak cycles are larger than the other records because these were near monotonic push cycles to the peak displacement while the crack distribution was still forming.

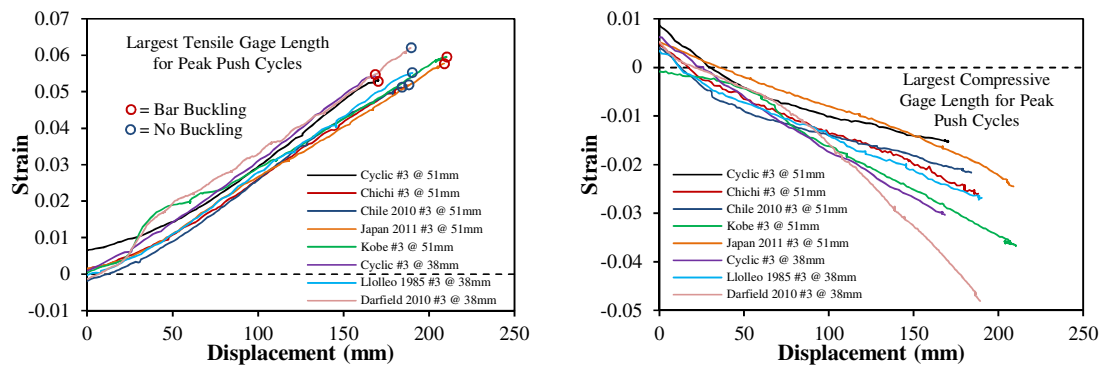


Figure 2.4. (Left) Relationship between Tensile Strain and Displacement during Peak Push Cycles of Load History Tests and (Right) Compressive Strain and Displacement during Peak Push Cycles

2.3 Transverse Steel Detailing and Bar Buckling

Five specimens with identical geometry, but varying transverse steel detailing were subjected to symmetric three cycle set load histories. The following transverse volumetric steel ratios were investigated: $4A_{sp}/(D's) = 0.5\%$ ($6d_{bl}$), 0.7%, 1%, and two separate detailing arrangements for 1.3%. In its current form, the symmetric three cycle set includes large increments between cycles which produced bar buckling in the experimental tests. Columns detailed with volumetric ratios 0.5% and 0.7% buckled reinforcement during displacement ductility six while columns containing 1% and 1.3% transverse steel produced bar buckling during ductility eight. An argument can be made that incremental ductility levels 5, 7, and 9 should be included in the load history. The relationship between strain and displacement does not seem to be affected by transverse steel detailing.

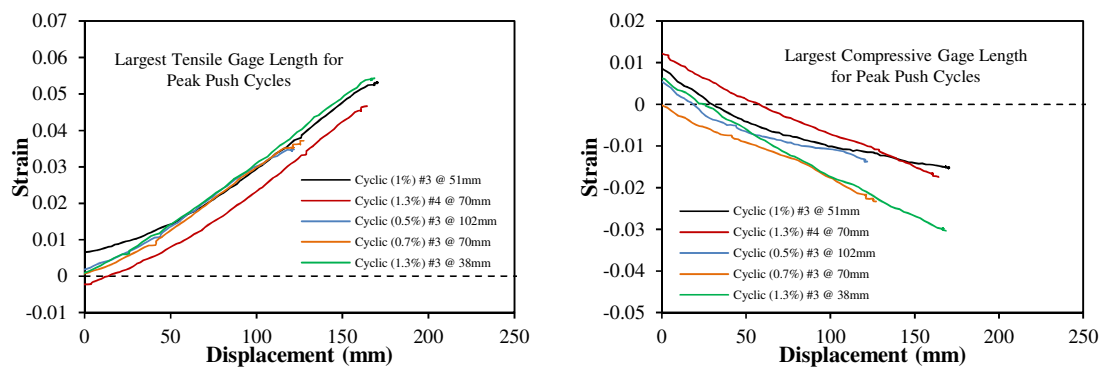


Figure 2.5. (Left) Relationship between Tensile Strain and Displacement during Peak Push Cycles of Transverse Steel Detailing Tests and (Right) Compressive Strain and Displacement during Peak Push Cycles

3. SPREAD OF PLASTICITY

3.1 Case Study: Deformation Components of Three Cycle Set Test with #3 Spiral at 38mm

The Optotrak instrumentation system allows a closer look at column flexure and strain penetration deformation components. To describe the process and capabilities of the system, sample test results related to the spread of plasticity in a symmetric three cycle set load history are presented. The displacement history along with data points which mark cycles where cover crushing and bar fracture occurred and cycles which produced visible bar buckling after reversal of loading appear in Fig. 3.1. The measured compressive and tensile strains for South and North extreme fiber bars during push cycles appear in Fig 3.1. This figure shows strain profiles for each extreme fiber bar to illustrate the effects of tension shift. The reinforcing bars contain thirty-two separate approximate 38mm gage lengths which appear as a single data point at its center linked to adjacent gage lengths with straight lines. Due to the effects of tension shift, compressive strains are concentrated near the column base and tensile strains are fanned out to a greater height following inclined crack distribution (Park and Paulay (1975)). Near the footing cracks remain effectively horizontal, but above this base section the flexural shear cracks are inclined. The tensile strains at the beginning of an inclined flexural shear crack do not coincide with the perceived moment demand at that location based on its height above the footing and the applied lateral load.

The measured strains of six reinforcing bars are plotted along the cross section to obtain curvatures in Fig. 3.2. The curvature was taken as the slope of the least squared error line. Curvature profiles obtained from thirty-two horizontal cross sections at different heights above the footing appear in Fig. 3.2. The measured linear plastic curvature distribution agrees with observations presented in (Hines, Restrepo, and Seible (2004)). The dashed lines for each curvature distribution represent a least squared error linear fit to the plastic portion of the measured curvatures. The extent of plastic curvatures above the footing may be calculated by determining where the linear plastic curvature distribution intersects the triangular yield curvature distribution, shown as a grey dashed line.

The target marker on each bar placed closest to the footing-column interface can be used to measure the effects of strain penetration. Development of fully anchored column longitudinal bars into the footing leads to bar slips along the partially anchored region of the bar near the footing-column interface, (Zhao and Sritharan (2007)). This slip is not a pull-out of the entire bar embedment length resulting from poor bond between the concrete and reinforcing bar. If the measured slips of the target markers are plotted along the cross section, the fixed-end rotation attributable to strain penetration may be calculated as the slope of a least squared error line, Fig. 3.3.

The hysteretic response in Fig. 3.3 was obtained from a string potentiometer at the center of load which measured the top column deflection. This total deformation is the addition of the column flexure, column shear, and strain penetration components. The flexural displacement may be determined by integrating the measured curvature distribution and adding the strain penetration deformation component. The curvatures above the instrumented region are assumed to follow the triangular yield curvature distribution. The strain penetration deformation component is equal to the measured fixed-end rotation multiplied by the clear column height. The integrated displacements from the Optotrak system are compared to the measured string potentiometer displacements in Fig. 3.3. The good agreement suggests that the shear deformation component is small relative to the total deformation.

The measured compression strains in the South reinforcing bar, see Fig. 3.1, are larger above the base section where several layers of transverse steel entered the inelastic range as shown in Fig. 3.4. The spiral layer closest to the footing-column interface remained elastic due to the additional confinement provided by the footing. Three layers of transverse steel entered the inelastic range during displacement ductility six, but bar buckling did not occur until reversal from tensile strains sustained during the first pull cycle of ductility eight. The outward buckled region of the South extreme fiber bar occurred over the previously inelastic transverse steel layers, see Fig. 3.1.

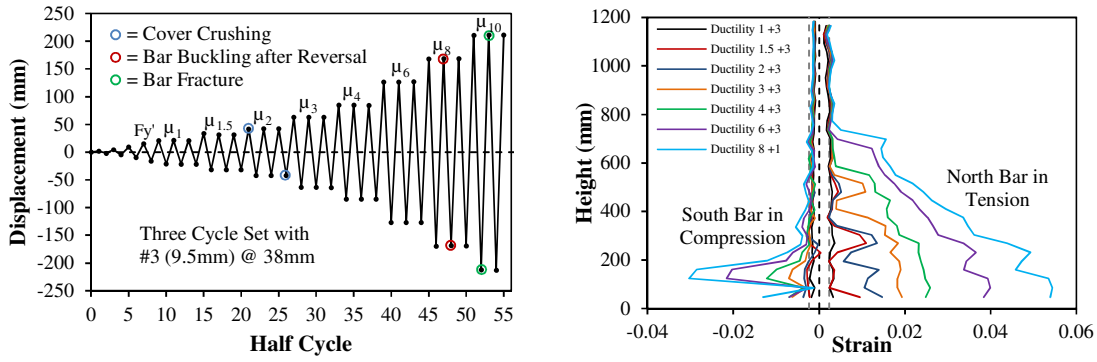


Figure 3.1. (Left) Symmetric Three Cycle Set Load History for Specimen with #3 (9.5mm) Spiral @ 1.5" and (Right) Vertical Strain Profiles for Both Extreme Fiber Bars during Push Cycles

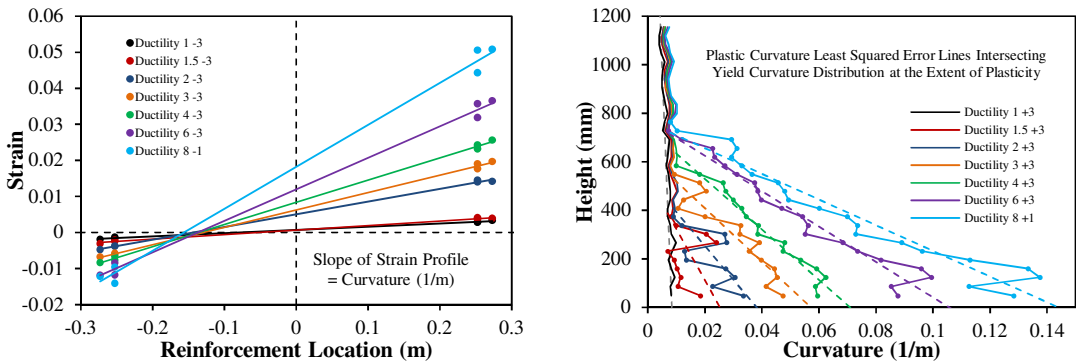


Figure 3.2. (Left) Cross Section Curvature Calculation and (Right) Vertical Curvature Profiles

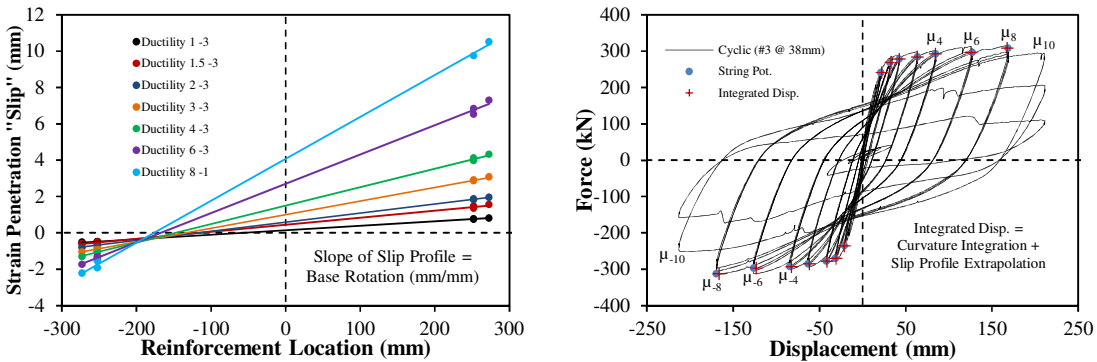


Figure 3.3. (Left) Base Rotation due to Strain Penetration and (Right) Measured and Integrated Displacements

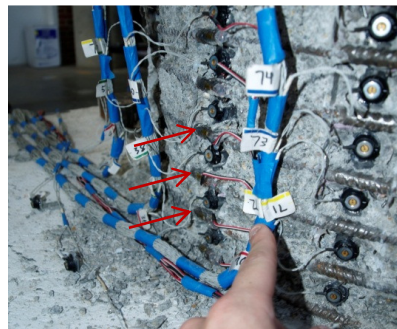
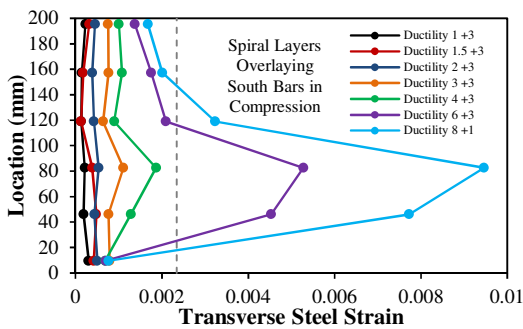


Figure 3.4. (Left) Spiral Strains on Compression Side and (Right) Extreme Fiber South Buckled Bar

3.2 Measured Spread of Plasticity

Plastic curvature profiles have a linear distribution which intersects the yield curvature profile at a height above the footing termed the extent of plasticity. This process is shown visually in the curvature profiles for a symmetric three cycle set load history with a #4 (12.7mm) spiral at 70mm on center in Fig. 3.5. For this test, the transverse steel remained elastic prior to bar buckling, and the measured curvatures closely follow a linear distribution. The measured extent of plasticity vs. base curvature ductility appears in Fig. 3.5. The spread of plasticity for column tests with varying geometry and predictive equations for the extent of plasticity appear in (Hines, Restrepo, and Seible (2004)). The column variables in Fig. 3.5 include load history and transverse steel detailing. The bi-linear relationship presented is expected to change for future tests which will focus on axial load ratio, aspect ratio, and longitudinal steel content.

The measured base rotation attributable to strain penetration is plotted against the base curvature ductility in Fig. 3.6. Equivalent strain penetration lengths are determined by dividing the measured fixed-end rotations by the base curvatures in Fig. 3.6. The top column displacement attributable to strain penetration is equal to the base curvature multiplied by the equivalent strain penetration length multiplied by the column clear height. A constant equivalent strain penetration length appears suitable for the range of curvature ductility in Fig. 3.6. This relationship is expected to change in future tests focusing on longitudinal steel content. A plastic hinge method which utilizes a response level dependent plastic hinge length is under development pending results of future tests. The goal is to improve the prediction of the relationship between strain and displacement to allow for accurate limit state target displacements. The limit state target displacements may be incorporated into a displacement-based design procedure to achieve a specific level of performance under a specific seismic hazard, (Priestley, Calvi, and Kowalsky (2007)).

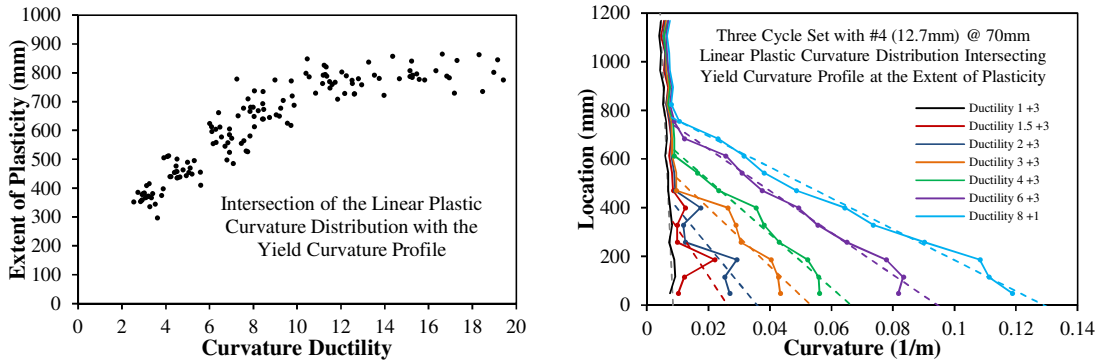


Figure 3.5. (Left) Measured Spread of Plasticity above the Footing-Column Interface and (Right) Extent of Plasticity Obtained from Curvature Profiles

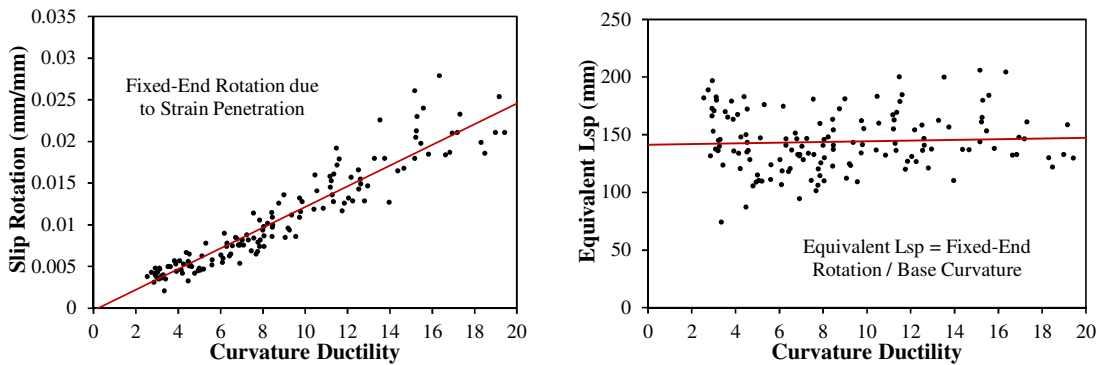


Figure 3.6. (Left) Base Rotations due to Strain penetration and (Right) Equivalent Strain Penetration Lengths

4. RESULTS

Results have shown that the damage control steel tensile strain limit was influenced by load history, but the relationship between strain and displacement was not. Specific earthquake time-history response characteristics were evaluated including: the number and amplitude of cycles prior to the peak, degree of symmetry, and peak displacement in each direction of loading. The symmetric three cycle set load history is more severe than the displacement history produced by real earthquakes, when evaluated to the same peak displacement, because of the high number of inelastic reversals of loading of increasing magnitude. The earthquake load histories needed to be scaled to larger displacements to produce bar buckling. Large inelastic strains, caused by large concrete compressive demand, decreased the effectiveness of the transverse steel in restraining buckling of the longitudinal bars. Plastic curvatures followed a linear distribution and as curvature ductility increased, the extent of plasticity stretched higher above the footing. Improvements to the moment curvature prediction for the relationship between strain and displacement can be made by taking into account the curvature ductility dependent linear distribution of plastic curvatures.

ACKNOWLEDGEMENT

The authors wish to acknowledge Alaska DOT&PF and Alaska University Transportation Center (AUTC) who supported this research through a series of grants. Special acknowledgement goes to Elmer Marx of Alaska DOT&PF who was closely involved in this research as the primary technical contact. The assistance of the entire staff of the Constructed Facilities Laboratory is appreciated.

REFERENCES

- Berry, M. P. and Eberhard, M. O. (2005). Practical Performance Model for Bar Buckling. *Journal of Structural Engineering* **131:7**, 1060-1070.
- Feng, Y., Kowalsky, M.J., and Nau, J.M. (2012). Fiber Model Investigating the Effect of Load History on Behavior of RC Bridge Columns. *Proceedings of the 15th World Conference on Earthquake Engineering*.
- Freytag, D. (2006). Bar buckling in reinforced concrete bridge columns. Master's thesis, University of Washington.
- Hines, E.M., Restrepo, J.I., and Seible, F. (2004). Force-Displacement Characterization of Well Confined Bridge Piers. *ACI Structural Journal* **101:4**, 537-548.
- Kunnath, S., El-Bahy, A., Taylor, A., and Stone, W. (1997). Cumulative Seismic Damage of Reinforced Concrete Bridge Piers. Technical Rep. NCEER-97-0006, National Center of Earthquake Engineering Research, Buffalo, N.Y.
- Moyer, M. J. and Kowalsky, M. J. (2003). Influence of Tension Strain on Buckling of Reinforcement in Concrete Columns. *ACI Structural Journal* **100:1**, 75-85.
- Park, R. and Paulay, T., (1975). Reinforced Concrete Structures. Wiley, New York.
- Priestley, M. J. N., Seible, F., and Calvi, G. M. (1996). Seismic Design and Retrofit of Bridges. John Wiley & Sons, New York.
- Priestley, M. J. N., Calvi, G. M., and Kowalsky, M. J. (2007). Displacement-Based Seismic Design of Structures. IUSS Press, Pavia, Italy.
- SEAOC (1999). Recommended Lateral Force Requirements and Commentary (7th Edition). Structural Engineers Association of California, Seismology Committee: Sacramento, CA.
- Scott, M. H. and Fenves, G. L. (2006). Plastic Hinge Integration Method for Force-Based Beam-Column Elements. *Journal of Structural Engineering* **132:2**, 244-252.
- Syntzirma, D. V., Pantazopoulou, S. J., Aschheim, M. (2010). Load-History Effects on Deformation Capacity of Flexural Members Limited by Bar Buckling. *Journal of Structural Engineering* **136:1**, 1-11.
- Zhao, J. and Sritharan, S. (2007). Modeling of Strain Penetration Effects in Fiber-Based Analysis of Reinforced Concrete Structures. *ACI Structural Journal*. **104:2**, 133-141.